Universidade de Aveiro Departamento de Engenharia Cerâmica e do Vidro
2009

Alexander Markevich

Cálculo por primeiros princípios de barreiras de difusão para pequenos agregados de lacunas em silício

Ab-initio calculations of diffusion barriers of small vacancy clusters in silicon

Dissertação apresentada à Universidade de Aveiro em cumprimento dos requisitos necessários à atribuição do grau de Mestre em Ciência e Engenharia de Materiais no âmbito do Programa Conjunto do Mestrado Europeu em Ciência dos Materiais sob a supervisão do Doutor José Pedro de Abreu Coutinho, Investigador Auxiliar no I3N – Universidade de Aveiro e co-supervisão do Professor Doutor Ryszard Pyrz, Professor Catedrático do Departamento de Engenharia Mecânica da Universidade de Aalborg.

A dissertation presented to the University of Aveiro in fulfilment of the requirements for the awarding of the Master degree in Materials Science and Engineering within the Joint European Masters Programme in Materials Science carried out under the supervision of Doctor José Pedro de Abreu Coutinho, Assistant Researcher at I3N – University of Aveiro, and co-supervision of Professor Ryszard Pyrz, Full Professor of the Department of Mechanical Engineering of Aalborg University.

Financial Support of European Consortium of Innovative Universities (ECIU) within the Joint European Masters Programme in Materials Science.

O Júri

Presidente

Prof. Dr. Vítor José Babau Torres
Professor Catedrático da Universidade de Aveiro

Prof. Dr. Ricardo Pedro Lopes Martins Mendes Ribeiro
Professor Auxiliar da Universidade do Minho

Dr. José Pedro de Abreu Coutinho
Investigador Auxiliar da Universidade de Aveiro (Orientador)

Acknowledgements

This Master thesis has been performed within the Joint European Masters Programme in Materials Science. First of all I would like to express my gratitude to the European Consortium of Innovative Universities (ECIU) for providing me with the opportunity to study at the University of Aveiro (UA) in Portugal and at the Hamburg University of Technology (TUHH) in Germany and for their financial support.

I am very grateful to my supervisor, Dr. José Coutinho, for his guidance during all the work on this Master project and for his friendly support during the time I have spent in Portugal. I would like to thank very much to my co-supervisor Ryszard Pyrz from Aalborg University, Denmark, for his assistance and support.

A lot of thanks to all professors from UA and TUHH, who tought me during this Master course, for their academic professionalism and overall support, especially to Prof. Margarida Almeida, Prof. Vitor Torres, Prof. Nikolai Sobolev, Prof. Vitor Amaral and Prof. Helena Nogueira.

Many thanks to my father, Dr. Vladimir Markevich, for providing me the insight into experimental physics and for his strong encouragement.

And finally I would like to thank all students of our Master course for their friendship. From them I have learnt a lot about different cultures and understood the versatility of our world.

Palavras chave Silício, Lacuna, Bi-lacuna, Tri-lacuna, Difusão, Modelação.

Resumo

Esta tese apresenta os resultados de um programa de investigação sobre a difusão da lacuna, bi-lacuna e tri-lacuna em silício utilizando simulações numéricas pelo método da teoria do funcional da densidade. Este método está implementado na forma de um programa informático referido como AIMPRO (Ab Initio Modelling PROgram). Para o cálculo dos pontos cela dos mecanismos de difusão foi usado o método “Nudged Elastic Band”.

As condições fronteira dos problemas foram impostas recorrendo à utilização de agregados esféricos de silício com 275 atomos, cuja superfície foi saturada por ligações Si-H. As lacunas foram então introduzidas no centro destes agregados. Os valores calculados das barreiras de difusão para a lacuna simples e para a bi-lacuna são respectivamente 0.68 e 1.75 eV. Estes valores apresentam um acordo razoável com os obtidos experimentalmente e obtidos em outros cálculos anteriores. A barreira de difusão da tri-lacuna foi, de acordo com a literatura disponível, calculada pela primeira vêz. O mecanismo de difusão mais favorável apresenta uma barreira de 2.2 eV. No seguimento dos resultados para a lacuna e bi-lacuna, pensamos que este resultado sobrestima a barreira em cerca de 0.25 eV, colocando a nossa melhor estimativa em 1.9-2.0 eV. Varias fontes de erro nos resultados são comentadas, assim como são sugeridas várias formas de as evitar.

Keywords Silicon, vacancy, divacancy, trivacancy, diffusion, modelling.

Abstract

This work presents the results of a computational investigation into the diffusion of the single vacancy (V) and small vacancy clusters, divacancy (V_2) and trivacancy (V_3), in silicon. The calculations were performed principally using local density functional theory as implemented by the AIMPRO (Ab Initio Modelling PROgram) code. The Nudged Elastic Band Method was used for elucidating diffusion paths and obtaining the energy barriers for diffusion of the defects considered.

Based on ab-initio calculations with H-terminated Si clusters with 275 host atoms, diffusion paths for neutral V_n (n = 1 to 3) defects were found. Calculated values of the activation energy for the diffusion of the Si vacancy and divacancy are 0.68 and 1.75 eV, respectively. These values are in a reasonable agreement with those derived from experimental and previous ab-initio modelling studies. The diffusion of trivacancy in Si has been modelled for the first time. The diffusion barrier of V_3 along the proposed diffusion path was found to be about 2.2 eV. This result comes overestimated as the experimental data indicates that the values of diffusion barriers for divacancy and trivacancy in Si should be similar. Probable sources of the calculation errors have been considered and possible ways to surmount these difficulties are proposed.

CONTENTS

LIST OF FIGURES **2**
LIST OF TABLES **2**
INTRODUCTION **3**
1. BACKGROUND THEORY **5**
1.1. The Many Body Problem 5
1.2. The Born-Oppenheimer Approximation 6
1.3. Density Functional Theory 7
1.3.1. Kohn-Sham Approach 8
1.3.2 Local Density Approximation 10
1.4. Pseudopotentials 10
2. DETAILS OF CALCULATIONS **12**
2.1. Choice of Boundary Conditions 12
2.2. The Cluster Implementation of AIMPRO 13
2.3. Calculation of diffusion barriers 15
2.3.1. Nudged Elastic Band Method 15
3. DIFFUSION OF SMALL VACANCY CLUSTERS IN SILICON **18**
3.1. Details of Nudged Elastic Band Method Implementation 18
3.2. Single Vacancy 18
3.2.1. Introduction 18
3.2.2. Results of calculations and their discussion 20
3.3. Divacancy 23
3.3.1. Introduction 23
3.3.2. Results of calculations and their discussion 25
3.4. Trivacancy 28
3.4.1. Introduction 28
3.4.2. Results of calculations and their discussion 29
SUMMARY **34**
REFERENCES **36**

LIST OF FIGURES

1 A single vacancy in Si……..... 19

2 Convergence of the Nudged Elastic Band Method for calculations of the single vacancy diffusion....……. 21

3 Minimum energy path for the single vacancy diffusion……..... 22

4 Positions of the Si host atoms near the vacancy for the initial and final states and the saddle point for diffusion…… 23

5 Divacancy with its six neighbouring host atoms in Si. b) Splitting of energy levels of divacancy in Si due to Jahn-Teller distortion…… 24

6 Total energy variation along the diffusion path of a divacancy in the neutral charge state in Si……..... 26

7 Positions of the Si host atoms near the divacancy for the initial and final states and the saddle point for diffusion……. 27

8 Total energy variation along the diffusion path of a trivacancy in the neutral charge state in Si……..... 31

9 Positions of a moving Si atom along the diffusion path for V_3…… 31

10 Atomic configurations corresponding to four positions of travelling Si atom along the diffusion path for V_3……. 32

LIST OF TABLES

1 Comparison of lattice constant, bulk modulus and band gap energy of Si obtained from supercell and cluster calculations and from experiment……... 12

2 Comparison of energy barriers for diffusion of divacancy in Si, which were derived from experimental works and from DFT calculations…… 27

3 Calculated and experimental values of diffusion barriers for the neutral V_n defects (n=1,2,3) in silicon……..... 34

INTRODUCTION

Vacancies are the dominant intrinsic defects in many materials at high temperatures. Vacancies can also be created under non-equilibrium conditions by irradiation with high-energy protons, electrons, neutrons, or ions. It is well established now that in silicon, the main material of modern semiconductor electronics, the single vacancy (V) is mobile at cryogenic temperatures (~100 K). Vacancies in Si attract each other and form aggregates which affect the electrical and optical properties of the material in a variety of ways. The aggregates themselves can have deep levels in the gap and be electron-hole recombination centers. They can also be the precursors of extended defects and/or gettering centers for a range of impurities. Further, it is believed that small vacancy aggregates are found at the core of dislocations and are responsible for much of their electrical activity. So, understanding of the structural, electronic and dynamic properties of vacancy aggregates in silicon is very important for the technology of production of different Si-based electronic devices.

The aggregation of vacancies in Si proceeds through the diffusion of single vacancies as well as the diffusion of small vacancy clusters. Therefore, understanding of vacancy aggregation processes requires the detailed knowledge of mechanisms and energy barriers for the diffusion of the single vacancy and the smallest vacancy complexes, the divacancy (V_2) and trivacancy (V_3). In spite of extensive studies for many years even the diffusion mechanism of the single vacancy is still not well understood and is debatable [1,2]. Divacancies and trivacancies are thought to be mobile at temperatures exceeding 200 ^{o}C [3]. The energy barrier for the diffusion of V_2 was determined in a number of experimental studies [4-7], however, it should be mentioned that the obtained values are spread in a rather wide range from 1.0 eV to 1.5 eV. There is no any published data on the activation energy for diffusion of the Si trivacancy.

In this thesis the results of a computational investigation into diffusion of the Si vacancy and small vacancy clusters, V_2 and V_3, are presented. The calculations were performed using local density functional theory as implemented by the AIMPRO (Ab Initio Modelling PROgram) code. The Nudged Elastic Band Method [8-10] was used for elucidating diffusion paths and obtaining the energy barriers for diffusion of the defects considered.

The thesis consists of the introduction, three chapters and the summary. The first chapter deals with the fundamentals of the Density Functional Theory, on which the calculations performed are based. The second chapter gives a description of some details of calculations, which were carried out with the use of the AIMPRO code. In the third chapter the description of the calculations performed and discussion of results obtained are presented. It consists of several sections dealing with single vacancy, divacancy and trivacancy separately. Each of these sections starts from an overview of experimental and modelling results obtained on particular defect and reported in the literature by the time, which is followed then by a description of the modelling results of this work and their discussion. Finally, all the results obtained in the present work are reviewed and summarized in the final chapter – Summary.

1. BACKGROUND THEORY

Density Functional Theory (DFT) is a modern powerful approach to performing electronic structure calculations in solids from *first principles*, using only the atomic numbers and coordinates as input parameters. This section will outline the fundamentals of modern computational methods based on DFT. It starts from the definition of quantum mechanics many-body problem, applied to systems of atomic nuclei and electrons, and Born-Oppenheimer approximation, which allows to separate electronic and nuclear motion. Then the DFT itself together with the Kohn-Sham equations and Local Density Approximation (LDA) will be discussed. And, finally, the pseudopotential approximation will be considered.

1.1. The Many Body Problem

Quantum mechanical approaches provide the description of a system by the solution of the Schrödinger equation. In the absence of external fields the time-independent and non-relativistic Schrödinger equation can be written as

$$\hat{H}\Psi = E\Psi\,, \tag{1.1}$$

where Ψ is a wave function – a function of a system parameters providing its complete description, and E is the energy of the system state described by Ψ. The Hamiltonian $\hat{H}$ is the energy operator which for the system of atomic nuclei and electrons takes the form[1]

$$\begin{aligned}\hat{H} &= \hat{T}_e + \hat{T}_i + \hat{V}_{i-e} + \hat{V}_{e-e} + \hat{V}_{i-i} = \\ &= -\frac{1}{2}\sum_i \nabla_i^2 - \sum_a \frac{1}{2M_a}\nabla_a^2 - \sum_{i,a}\frac{Z_a}{|\mathbf{R}_a - \mathbf{r}_i|} + \frac{1}{2}\sum_{i,j:i\neq j}\frac{1}{|\mathbf{r}_i - \mathbf{r}_j|} + \frac{1}{2}\sum_{a,b:a\neq b}\frac{Z_a Z_b}{|\mathbf{R}_a - \mathbf{R}_b|}.\end{aligned} \tag{1.2}$$

[1] All quantities are expressed in atomic units (unless otherwise specified). In this system of units, $\hbar$, e, m and $4\pi\varepsilon_0$ are taken to be unity, where e, m and ε_0 are the electron charge, electron mass, and the permittivity of vacuum, respectively. The unit of length is 0.529 Å, and the unit of energy is 27.211 eV.

where M_a, Z_a, and $\mathbf{R}_a$ represents the mass, charge and position of the a-th nucleus, and $\mathbf{r}_i$ is the i-th electron coordinate. The first two terms in the Equation 1.2 represent the kinetic energies of the electrons and nuclei respectively, and the subsequent terms describe the electron-nuclear, electron-electron and inter-nuclear Coulomb interaction energies, respectively.

For the system of N_n atomic nuclei and N_e electrons the total wave function Ψ is a function of N_n nuclei coordinates, N_e electron and spin coordinates, $\mathbf{r}_i$ and s_i respectively,

$$\Psi \equiv \Psi(\mathbf{r}_1, s_1, ..., \mathbf{r}_{N_e}, s_{N_e}; \mathbf{R}_1, ..., \mathbf{R}_{N_n}), \tag{1.3}$$

The fact that the wave function depends on $4N_e+3N_n$ scalar variables makes the solution of the Schrödinger equation, in its actual form 1.1, intractable even when using the fastest computers available. The complexity of the problem is possible to reduce by adopting several approximations.

1.2. The Born-Oppenheimer Approximation

The large difference between the masses of electrons and nuclei makes it logical to assume that electrons respond instantaneously to nuclei motion. In other words, on the typical time-scale of the nuclear motion, the electrons will rapidly relax to the instantaneous ground-state configuration. Therefore it is possible to separate electronic and nuclear motion, and first solve Schrödinger equation for the electrons in the potential generated by the static nuclei and then solve for the nuclei where the electronic energy enters as a potential. This separation of electronic and nuclear motion is known as the Born-Oppenheimer approximation. The total wave function can then be written

$$\Psi(\mathbf{r}, \mathbf{R}) = \phi(\mathbf{R})\psi(\mathbf{r}; \mathbf{R}), \tag{1.4}$$

where $\psi(\mathbf{r};\mathbf{R})$ and $\phi(\mathbf{R})$ are the separate electronic and nuclear wave functions. The variables $\mathbf{r}$ and $\mathbf{R}$ represent the space coordinates of all electrons ($\mathbf{r}_1$, $\mathbf{r}_2$, $\mathbf{r}_3$,…) and all nuclei ($\mathbf{R}_1$, $\mathbf{R}_2$, $\mathbf{R}_3$,…) respectively. The designation $\psi(\mathbf{r};\mathbf{R})$ stresses the fact that the electronic

wave function depends on nuclei coordinates **R** in a parametric way. The Schrödinger equation for the electrons can be written as

$$\hat{H}_e \psi(\mathbf{r};\mathbf{R}) = E_e(\mathbf{R})\psi(\mathbf{r};\mathbf{R}) \tag{1.5}$$

with Hamiltonian

$$\begin{aligned}\hat{H}_e &= \hat{T}_e + \hat{V}_{i-e} + \hat{V}_{e-e} = \\ &= -\frac{1}{2}\sum_i \nabla_i^2 - \sum_{i,a}\frac{Z_a}{|\mathbf{R}_a - \mathbf{r}_i|} + \frac{1}{2}\sum_{i,j:i\neq j}\frac{1}{|\mathbf{r}_i - \mathbf{r}_j|}.\end{aligned} \tag{1.6}$$

The dependence of the eigenvalues E_e in Equation 1.5 on the nuclear position **R** is acknowledged. Nuclear motion is usually neglected, but their positions can be varied in order to find the ground state of the whole system. The total energy will be then the sum of the energy of electrons $E_e(\mathbf{R})$ and the electrostatic energy of the nuclei.

Although the Born-Oppenheimer approximation considerably simplifies the Schrödinger equation, the problem still cannot be solved because of the inter-electronic interactions term. There are two main approaches that treat this problem, Hartree-Fock and Density Functional theories. Although they use different variational parameters, one-electron wave functions in Hartee-Fock and electronic charge density in DFT, these approaches reduce the many-electron problem to an uncoupled problem in which the interaction of one electron with the remaining ones is incorporated in an averaged way into a potential felt by the electron. The Schrödinger equation then becomes separable and the problem can be solved analytically.

1.3. Density Functional Theory

Density-functional theory (DFT) was introduced in 1964 by Hohenberg and Kohn [11] who showed that the ground-state of the system is uniquely determined by the electronic charge density $n(\mathbf{r})$. Therefore it is possible to solve the Schrödinger equation in

terms of $n(\mathbf{r})$. This is implemented in DFT by minimizing the total energy as a functional of electronic charge density

$$E_0 = \min_{\tilde{n}} E\left[\tilde{n}(\mathbf{r})\right], \tag{1.7}$$

where E_0 is the ground-state energy and $\tilde{n}(\mathbf{r})$ is a trial density. This expression is an interpretation of the energy variational principle. The total energy functional is defined as

$$E[n] = F[n] + \int v_{ext}(\mathbf{r}) n(\mathbf{r}) d^3\mathbf{r}\,, \tag{1.8}$$

where the functional F is universal (system-independent), and accounts for electronic kinetic energy, electron-correlation and exchange interactions. External potential v_{ext} to which the electrons are subject includes the ion-electron interaction and other external fields.

Adopting the charge density as the variational parameter will vastly simplify the computational procedure. Instead of dealing with the many electron wave function which depends at least on $3N$ variables (coordinates for each electron) for a system of N electrons, DFT uses the charge density which is only a function of three variables, x, y and z.

1.3.1. Kohn-Sham Approach

The idea proposed by Kohn and Sham [12] is that, even though it is not possible to write the functional $F[n]$ explicitly for the system of interacting electrons, we can treat this problem for the fictitious system of non-interacting electrons by adding the appropriate auxiliary external potential. The total energy functional can be written as

$$E[n] = T[n] + \int \frac{n(\mathbf{r}) n(\mathbf{r}')}{|\mathbf{r} - \mathbf{r}'|} d^3\mathbf{r} d^3\mathbf{r}' + \int v_{ext}(\mathbf{r}) n(\mathbf{r}) d^3\mathbf{r} + E_{xc}[n], \tag{1.9}$$

where $T[n]$ is defined as the kinetic energy of a non-interacting gas with the same density $n(\mathbf{r})$, the second and third terms are the electrostatic energies of the electron in the field of

the total electron density (Hartree energy) and of the static nuclei respectively, and the final term is the exchange-correlation energy that contains non-classical electrostatic interaction energy and the difference between the kinetic energies of the interacting and non-interacting systems. The aim of this separation is that the first three terms can be dealt with simplicity, and the last term, which contains the effects of the complex behaviour, is a small fraction of the total energy and often can be approximated quite well.

This approach leads to the following set of one-electron Schrödinger equations with an effective independent particle Hamiltonian

$$\left[-\frac{1}{2}\nabla^2 - \sum_a \frac{Z_a}{|\mathbf{r}-\mathbf{R}_a|} + \int \frac{n(\mathbf{r}')d^3\mathbf{r}'}{|\mathbf{r}-\mathbf{r}'|} + V_{xc}[n](\mathbf{r})\right]\psi_\lambda(\mathbf{r}) = \varepsilon_\lambda \psi_\lambda(\mathbf{r}) \tag{1.10}$$

with the density $n(\mathbf{r})$ obtained by summing up all occupied orbitals

$$n(\mathbf{r}) = \sum_\lambda |\psi_\lambda(\mathbf{r})|^2 . \tag{1.11}$$

The wave functions ψ_λ are known as Kohn-Sham orbitals and are only used to construct the charge density and should not be treated as one-electron wave functions.

The exchange-correlation potential $V_{xc}[n]$ is given by

$$V_{xc}[n](\mathbf{r}) = \frac{\delta E_{xc}[n]}{\delta n(\mathbf{r})} . \tag{1.12}$$

Equations 1.10 and 1.11 are known as Kohn-Sham equations and solved in a self-consistent loop. First the trial charge density is used to solve Equation 1.10. From the resulting eigenvectors a new charge density is calculated, following Equation 1.11, and used as a new input to Equation 1.10. This self-consistency cycle keeps going until the charge density does not change appreciably.

1.3.2 Local Density Approximation

The remarkable result of density-functional theory is the existence of an universal exchange-correlation energy functional $E_{xc}[n]$ which depends only on the electronic charge density, leading to the knowledge of the exact ground state energy and density. However the exact form of this functional is unknown. The most common approach to overcome this problem is the local density approximation (LDA). In the LDA the exchange-correlation energy is assumed to be local and takes the value it would have for the homogeneous electron gas with the same charge density.

$$E_{xc}[n] = \int \varepsilon_{xc}[n(\mathbf{r})] n(\mathbf{r}) d^3\mathbf{r}\,, \tag{1.13}$$

where $\varepsilon_{xc}[n(\mathbf{r})]$ is the exchange-correlation energy per electron in a homogeneous electron gas of density $n(\mathbf{r})$ [13].

The LDA is exact for a homogeneous electron gas and works well for systems with slowly varying density. However this is not usually the case, and several modifications for the exchange-correlation functional form are available. In this work we use the LDA exchange-correlation functional of Perdew and Wang (PW92) [14] along with a Padé parametrization [15].

1.4. Pseudopotentials

It is well known that the standard properties of molecules or solids are governed by valence electrons. The core electrons behave much like those in isolated atoms, thus their contribution to the total energy does not change when the isolated atoms are brought together to form a molecule or crystal. In the following approach the all-electron problem is replaced by a *pseudopotential* formalism which describes valence states accurately, whereas the core states are formally replaced by a set of functions. The valence electrons wave functions in Kohn-Sham equations are then should be also replaced by *pseudo-wave-functions* which give the correct charge density outside the core region. The use of pseudopotentials has several considerable advantages:

1. It provides a way to avoid calculating the wave functions of the core electrons, which considerably reduces computational efforts.
2. The exclusion of the core states results in a large lowering in the magnitude of the total energy therefore reduces errors when comparing similar systems.
3. Direct modelling of core electrons of heavy atoms would have to include relativistic effects, while valence electrons retain non-relativistic behaviour.

The pseudopotential for a certain atomic species can be used for different systems i.e. is transferable. This is a consequence of the *frozen core approximation* which assumes the core state to be unperturbed when the atom is transferred to a specific environment. Another approximation implicit in the use of pseudopotentials is the *small core approximation* where the overlap between core and valence state is assumed to be negligible.

In the calculations presented in this work the pseudopotential of Bachlet, Haman and Schluter (BHS) [16] are used. These pseudopotentials have several fundamental properties:

1. The real and pseudo-valence eigenvalues are equal for a chosen prototype atomic configuration.
2. Beyond a chosen core radius r_c the real and pseudo-atomic wavefunction agree exactly.
3. The integrated charge density is the same for both real and pseudo-charge densities for $r > r_c$ (norm conservation).
4. The first energy derivatives and logarithmic derivatives of the real and pseudo-wave function agree for $r > r_c$.

2. DETAILS OF CALCULATIONS

Almost all calculations presented in this work have been done using H-terminated atom-centred spherical cluster of 275 Si atoms. The outer Si-H units were kept fixed during the cluster relaxation. The basis sets for valence states are atom-centred *s*- and *p*-like Gaussian functions with four optimized exponents together with *d*-polarization functions. The Nudged Elastic Band method was used to find migration barriers of vacancy clusters.

This section is intended to explain the choice of these conditions and to describe the implementation details of AIMPRO. These include an explanation for the choice of boundary conditions, the specificity of the cluster implementation of the program, and a description of the Nudged Elastic Band method.

2.1. Choice of Boundary Conditions

Two different types of boundary conditions are usually employed to model lattice defects – *supercell* and *cluster*. A supercell is a volume of solid that repeats itself periodically in space. This is an exact representation of a perfect crystal. On the other hand, the cluster consists of a finite portion of solid whose surface is passivated, generally with hydrogen, to eliminate free radicals.

In Table 1 the lattice constant a_0, bulk modulus B and band gap energy E_g at 0 K of Si obtained from supercell and cluster calculations are compared with experimental values.

Table 1. The lattice constant a_0, bulk modulus B and band gap energy E_g at 0 K of Si obtained from supercell and cluster calculations and corresponding experimental values.

	a_0, Å	B, GPa	E_g, eV
Supercell	5.38	96.3	0.54
Cluster	5.39	–	2.5
Experiment [a]	5.43	97.9	1.17

[a] Ref. [46]. Bulk modulus is given at 296 K.

It is well known fact that DFT based supercell calculations underestimate the band gap energy. This occurs due to the approximation to the exchange-correlation energy employed within the LDA and due to the discontinuity in the exchange-correlation potential when an electron is added to the insulating system [17]. On other hand the cluster calculations are known to overestimate significantly the band gap energy as a result of a small size. With increasing the cluster size the band gap energy will decrease to that of the supercell methode, as a supercell represents the theoretical approach to the bulk crystal.

The choice between supercell and cluster is based on the specificity of the defect to be calculated. In the present work the cluster method is used for calculating the ground state energies and migration barriers of small vacancy clusters. The reason for this choice is that the lattice relaxations associated with large Jahn-Teller distortions [18], inherent in small vacancy clusters, have a long-ranged character [19]. These relaxations can be significantly altered by the interaction of the defects in neighbouring supercells, which leads to a wrong picture of the defect and significant errors in calculations. On the other hand, real-space cluster calculations are computationally less demanding, allowing us to consider about twice the number of host atoms, and therefore strain fields are better accounted for. Since the cluster is not large enough it is necessary to minimize the interaction of the defect with surface. This can be done by keeping the surface atoms fixed during structural optimizations, thus reproducing the pressure exerted by the host crystal. The relaxation at fixed volume also facilitates the comparison of different defect systems, that is crucial for calculations of relative energies and energy levels.

2.2. The Cluster Implementation of AIMPRO

In the cluster method the Kohn-Sham wave functions are expanded in a basis of localized orbitals $\phi_i(\mathbf{r}-\mathbf{R}_i)$ [20]

$$\psi_\lambda(\mathbf{r},s)=\chi_\alpha(s)\sum_i c_i^\lambda \phi_i(\mathbf{r}-\mathbf{R}_i)\,, \tag{2.1}$$

where $\chi_\alpha(s)$ are the spin functions and λ is a level index. In this way the Kohn-Sham differential equations are converted to matrix equations for c_i^λ. The localized orbitals are represented by Cartezian-Gaussian atom-centred functions in the form

$$\phi_i(\mathbf{r}-\mathbf{R}_i) = (x-\mathbf{R}_{ix})^{n_1}(y-\mathbf{R}_{iy})^{n_2}(z-\mathbf{R}_{iz})^{n_3} e^{-a_i(\mathbf{r}-\mathbf{R}_i)^2}, \tag{2.2}$$

where n_1, n_2 and n_3 are integers. If these are all zero, ϕ will be an *s*-type orbital of spherical symmetry. Orbitals of *p*-symmetry correspond to one of these integers being unity and the others zero. And if $n_1 + n_2 + n_3 = 2$ five *d*-type and one *s*-type orbitals will be generated. In this respect, this basis set is overcomplete. The advantage of using Gaussian type functions is that their related integrals can be analytically found.

The charge density for each spin is constructed in terms of a density matrix, $b_{\mathrm{ij,s}}$,

$$n_s(\mathbf{r}) = \sum_{i,j} b_{ij,s}\phi_i(\mathbf{r}-\mathbf{R}_i)\phi_j(\mathbf{r}-\mathbf{R}_j), \tag{2.3}$$

$$b_{ij,s} = \sum_{\lambda_{occ}} \delta(s,s_\lambda) c_i^\lambda c_j^\lambda, \tag{2.4}$$

where the sum is over occupied orbitals λ with spin *s*. The total charge density $n(\mathbf{r})$ can then be written as

$$n(\mathbf{r}) = \sum_s n_s(\mathbf{r}) = \sum_{i,j} b_{ij}\phi_i(\mathbf{r}-\mathbf{R}_i)\phi_j(\mathbf{r}-\mathbf{R}_j), \tag{2.5}$$

$$b_{ij} = \sum_s b_{ij,s}. \tag{2.6}$$

Each term of the energy will be calculated in the space defined by this basis. After solving Kohn-Sham equations, the self-consistent charge density will be obtained for a particular atomic configuration. This charge density yields the structural potential energy which is used to calculate the forces, acting on each atom in the system. The atoms are moved via a *conjugate gradient algorithm* until these forces vanish in the relaxation

process of the cluster. As a result a minimum system total energy will be achieved. In a defective cluster there may be several local energy minima that correspond to the different defect configurations. The lowest of them – the global minimum – corresponds to the most stable configuration.

2.3. Calculation of diffusion barriers

From the microscopic point of view the diffusion in solids is the result of a sequence of localized jumps of the diffusing atoms from one lattice site to another. Thus the diffusion rate D is proportional to the probability of successful atomic jump to occur, which is given by Boltzmann distribution, and can be written as

$$D = C\nu \exp\left(-\frac{Q}{k_B T}\right), \tag{2.7}$$

where C is the proportionality factor, ν is the attempt frequency, which is of the order of the Debye frequency, multiplied by the entropy factor, k_B is the Boltzmann constant, T is the temperature at which the diffusion process occur and Q is the activation energy of diffusion.

The activation energy is equal to the minimum energy barrier that diffusing atom should overcome to move from one stable position to a neighbouring equivalent one. This barrier corresponds to the maximum on the potential energy surface – saddle point – along the minimum energy path (MEP) between two neighbouring stable configurations. The computational procedure to define the diffusion barrier is then consists in finding the MEP and calculating the energy of the saddle point.

2.3.1. Nudged Elastic Band Method

The Nudged Elastic Band (NEB) is an efficient method to find a lowest energy reaction pathway, or minimum energy path (MEP), between a given initial and final stationary state [8-10]. The potential energy maximum along the MEP is the saddle point

energy which gives the activation energy barrier. The NEB method has been successfully used to find the mechanism and activation energy for diffusion of different defects in semiconductors [21, 22].

NEB is a chain-of-states method in which a string of images of the system is constructed to form a discrete representation of the reaction path. Each "image" corresponds to a specific geometry of the atoms on their way from the initial to the final configuration. These images are connected together by “springs”, representing an elastic band, to ensure the continuity of the path. The initial path (or string of images) may be generated by the straight line interpolation between the end point configurations and all intermediate images are adjusted by optimization algorithm to bring the band to the MEP. The optimization involves minimization of the force acting on the images.

In the elastic band method, the total force acting on an image is the sum of the potential force, or true force, and the spring force $\mathbf{F}_i^s$,

$$\mathbf{F}_i = -\nabla V(\mathbf{R}_i) + \mathbf{F}_i^s , \tag{2.8}$$

where $\nabla V(\mathbf{R}_i)$ is the gradient of the energy with respect to the atomic coordinates $\mathbf{R}_i$ in the system at image *i*.

The essential feature of the NEB method is that only the perpendicular component of the true force and parallel component of the spring force are used to move the atoms. This force projection is referred to as “nudging”. The force on image *i* becomes

$$\mathbf{F}_i^{NEB} = -\nabla V(\mathbf{R}_i)\,|_{\perp} + \mathbf{F}_i^s\,|_{\|}, \tag{2.9}$$

where the true force is given by

$$\nabla V(\mathbf{R}_i)\,|_{\perp} = \nabla V(\mathbf{R}_i) - \nabla V(\mathbf{R}_i)\cdot\hat{\boldsymbol{\tau}}_i\hat{\boldsymbol{\tau}}_i \tag{2.10}$$

and the spring force

$$\mathbf{F}_i^s\,|_{\|} = k(|\,\mathbf{R}_{i+1} - \mathbf{R}_i\,| - |\,\mathbf{R}_i - \mathbf{R}_{i-1}\,|)\cdot\hat{\boldsymbol{\tau}}_i , \tag{2.11}$$

where k is the spring constant and $\hat{\boldsymbol{\tau}}_i$ is the unit tangent to the path at each image which is defined as

$$\hat{\boldsymbol{\tau}}_i = \boldsymbol{\tau}_i \Big/ |\boldsymbol{\tau}_i| \tag{2.12}$$

$$\boldsymbol{\tau}_i = \frac{\mathbf{R}_i - \mathbf{R}_{i-1}}{|\mathbf{R}_i - \mathbf{R}_{i-1}|} + \frac{\mathbf{R}_{i+1} - \mathbf{R}_i}{|\mathbf{R}_{i+1} - \mathbf{R}_i|} \tag{2.13}$$

This force projection scheme decouples the relaxation of the path and the discrete representation of the path. The spring forces only control the spacing of the images along the band and do not interfere with the convergence of the elastic band to the MEP, as well as the true force does not affect the distribution of images along the MEP. This ensures that each image finds the lowest energy possible while maintaining a reasonable spacing between neighbouring images.

3. DIFFUSION OF SMALL VACANCY CLUSTERS IN SILICON

3.1. Details of Nudged Elastic Band Method Implementation

For modelling diffusion pathways and calculation of migration barriers the NEB implementation of AIMPRO has been used (see section 2.3). A set of system images generated by a linear interpolation between initial and final atomic configurations represent the first approximation for the diffusion path. The end configurations were firstly relaxed to the minimum energy states, and they are not optimized during the NEB algorithm realization. During the image relaxations all atomic positions, except the outer Si-H units, were optimised.

There are two important parameters that characterise the realization of the NEB algorithm:

nopt – the number of structural optimisation iterations performed for each image during each *pass* of the band, and

passes – the number of *passes* over the entire chain. After each *pass* is finished the elastic band forces are updated.

The total number of optimizations will be *nimage*×*nopt*×*passes*, where *nimage* is the number of optimized images of the system. These parameters can be varied with respect to the problem specificity. It is important to choose enough images to represent the path correctly and to make the number of optimizations for each image large enough to obtain the convergence of the elastic band to the MEP. As a result the calculations become extremely time consuming. And even for modelling the single vacancy diffusion path with five images to be relaxed, the convergence to the MEP takes several weeks on a desktop computer.

3.2. Single Vacancy

3.2.1. Introduction

The structural and electronic properties of the single vacancy (V) in silicon were first indentified by electron-paramagnetic-resonance (EPR) measurements [23-25]. It was

demonstrated that the single vacancy in Si introduces four levels into the band gap, i.e. it can take on five different charge states, from the doubly positively charged state to the doubly negatively charged one (V^{2+}, V^{+}, V^{0}, V^{-}, V^{2-}). Undistorted monovacancy posses the T_d symmetry and induces a singlet (a1) level in the valence band manifold and a triplet (t2) level inside the band gap. The degeneracy associated with occupying the t2 level results in the high lattice distortion by the dangling bond reconstructions and changing the defect symmetry (Jahn-Teller effect), T_d (V^{2+}) → D_{2d} (V^{+}, V^{0}) → C_{2v} (V^{-}). Bond reconstructions are associated with pairing four Si atoms around the vacancy by forming weak covalent bonds. This effect was observed experimentally [23-25] and investigated by ab-initio calculations [19,26,27]. It was shown that lattice relaxations, associated with large Jahn-Teller distortion, have an anisotropic and long-ranged character [19]. These relaxations mainly propagate along the zigzag chains of atoms that contain the vacant site. One of the results of a strong Jahn-Teller distortion is a reversed ordering of donor levels [26,28], a phenomenon known as negative electron correlation energy, "negative U" [29]. The atomic structure of the monovacancy with its four nearest neighbour atoms is shown in Fig. 1. The pairing distortion of Si atoms and formation of new covalent bonds are also depicted.

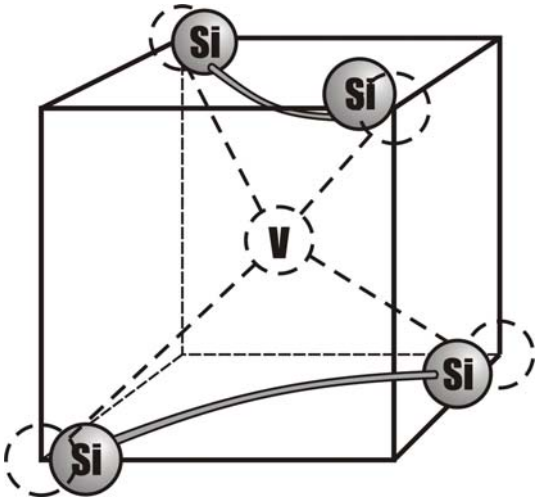

Fig. 1. A single vacancy with its four neighbouring host atoms in Si. The pairing distortion of Si atoms and formation of new covalent bonds are sketched.

The vacancy become mobile at ~70 K in n-type (V^{2-}), ~150 K in p-type (V^{2+}) and ~200 K in high resistivity material (V^{0}) and readily forms complexes with other defects

such as other vacancies and impurities [24,25]. The trapping of a vacancy by impurities was successfully used for investigation of the vacancy diffusion. The EPR and DLTS studies gave the values of activation energies 0.18±0.02 eV, 0.45±0.04 eV and 0.32±0.02 eV for V^{2-}, V^{0} and V^{2+} respectively. The strong dependence of the activation energy for migration on the charge state of the vacancy can be explained by the strong lattice relaxation associated with the broken bonds reconstruction versus charge state (Jahn-Teller effect).

Such low activation energies for migration imply that single vacancy is very mobile, which makes it difficult to detect experimentally. The conventional method, successful for many materials, of quenching in vacancies for study by rapid cooling from high temperatures does not work for silicon, the material cannot be quenched rapidly enough to freeze in a measurable concentration of vacancies. Therefore the only successful method for isolated vacancy production for studying is by irradiation at cryogenic temperatures.

In a recent critical evaluation of experimental and theoretical results on the vacancy in silicon the activation energy for vacancy contribution to self-diffusion was estimated to be 4.5-4.6 eV [2]. Combining this with the activation energy for vacancy migration, the formation energy of the lattice vacancy in silicon comes about 4.0 eV. This value was supported by positron-lifetime experiments [30] and is in agreement with recent DFT calculations, 3.98 eV [31].

3.2.2. Results of calculations and their discussion

The mechanism of diffusion of the single vacancy at low temperatures is just hopping of the vacancy between neighbouring lattice sites. In other words, a neighbour Si atom makes a jump to the vacant site, thus the atom and the vacancy exchange their positions. A set of seven images was used to represent the diffusion path of the single vacancy in our calculations. The initial position corresponds to the vacancy in the centre of the cluster. There are four possibilities for the final position that correspond to the exchange of the vacancy with one of the four neighbouring Si atoms. These positions are absolutely identical as a consequence of the lattice symmetry. The ground state energies of the fully relaxed initial and final configurations differ by 0.054 eV, and this is caused by

the defect-surface interaction. Because of the defect-surface interaction, all positions of the vacancy, that are not symmetrical relative to the cluster centre, have slightly different ground state energies. This effect becomes more pronounced when the defect approaches the surface of the cluster.

Fig. 2 represents the rate of convergence of the elastic band of images from the initial approximation to the MEP. About 40 structural optimizations for each image (200 for the chain) are needed to approach the MEP. But in order to make the total forces acting on each image (Eq. 2.8) negligible (which means the full convergence to the MEP), 112 structural optimizations for each image (560 for the chain) have to be performed. The convergence rate varies for calculations of different problems and usually decreases with increasing complexity of a problem.

The calculated energies for each image of the system, relative to the energy of the initial position, are shown in Fig. 3. This graph represents the MEP for the single vacancy diffusion.

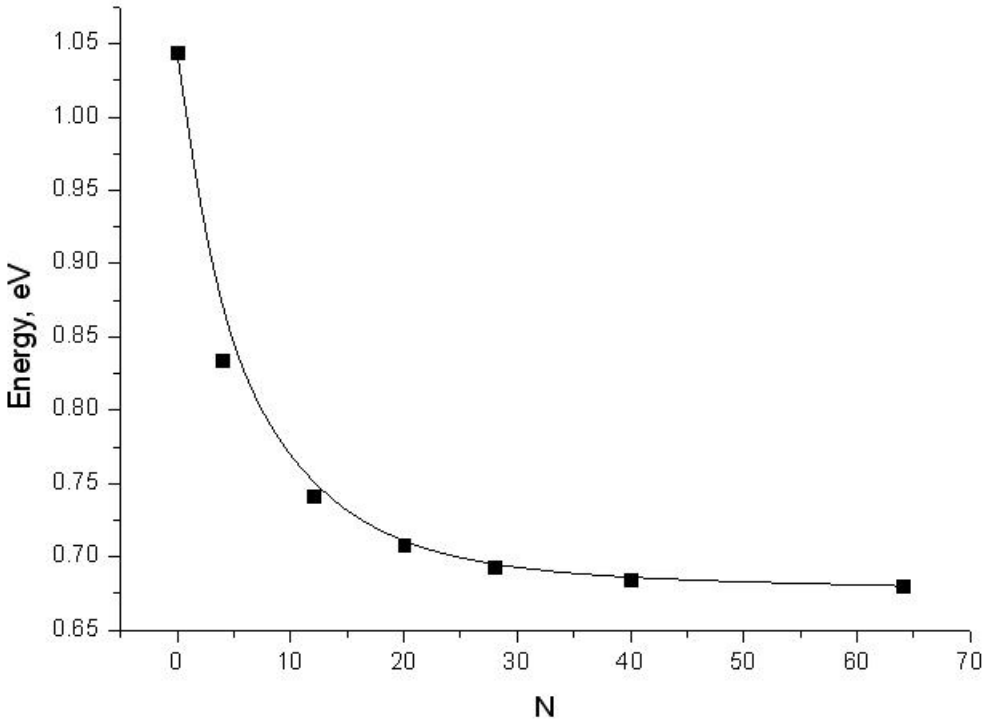

Fig. 2. Convergence of the elastic band of images from the initial approximation to the MEP. Y-axis represents the saddle point energy, and x-axis represents number of structural optimizations performed on each image.

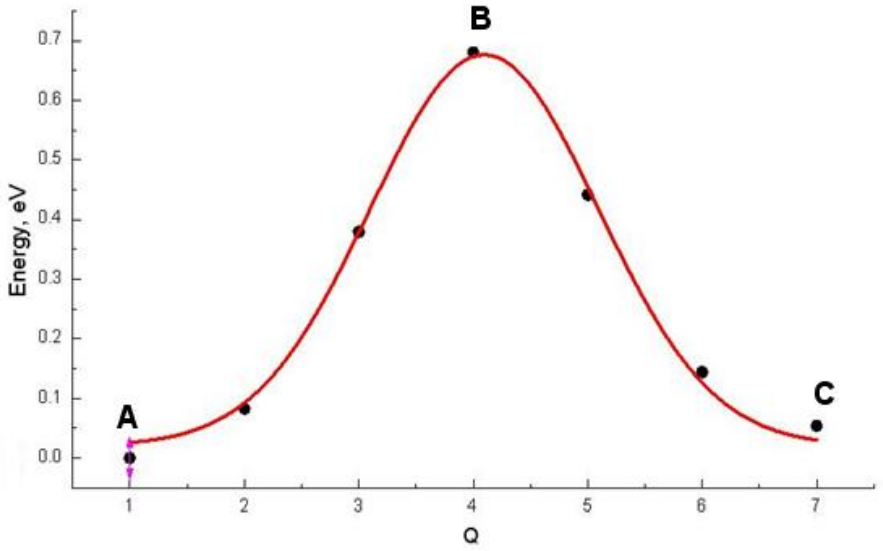

Fig. 3. Minimum energy path for the single vacancy diffusion. Black circles represent calculated energies, relative to the energy of the initial position, for each image of the system. The red solid line is an interpolation, which is shown as a guide for eyes. *Q* is a NEB image's number and represents the distance (arbitrary units) from the initial position. Positions A, B and C correspond to the atomic configurations shown in Fig. 4.

The saddle point was found to be the configuration when the Si atom lies midway between two vacant sites, Fig. 4B. The diffusion barrier – the energy difference between the initial configuration and the saddle point – was calculated to be 0.68 eV for the neutral charge state of the vacancy. According to the most reliable experimental studies [24,25], the barrier for the diffusion of neutral vacancy should be 0.45 ± 0.04 eV. So, it appears that the obtained calculated value is overestimated. There might be a few possible reasons for the overestimation. First, cluster calculations are known to overestimate the band gap energy that has already been mentioned in section 2.1. This allows one-electron levels to vary widely between ground state and saddle point configurations, and energy difference may result overestimated. Second, the long range atomic relaxations, associated with Jahn-Teller distortion of four nearest Si atoms, may cause a significant effect of defect-surface interactions, which will prohibit the full relaxations of the images. It is very difficult to determine the contributions of these effects to total errors in calculations of energy barriers.

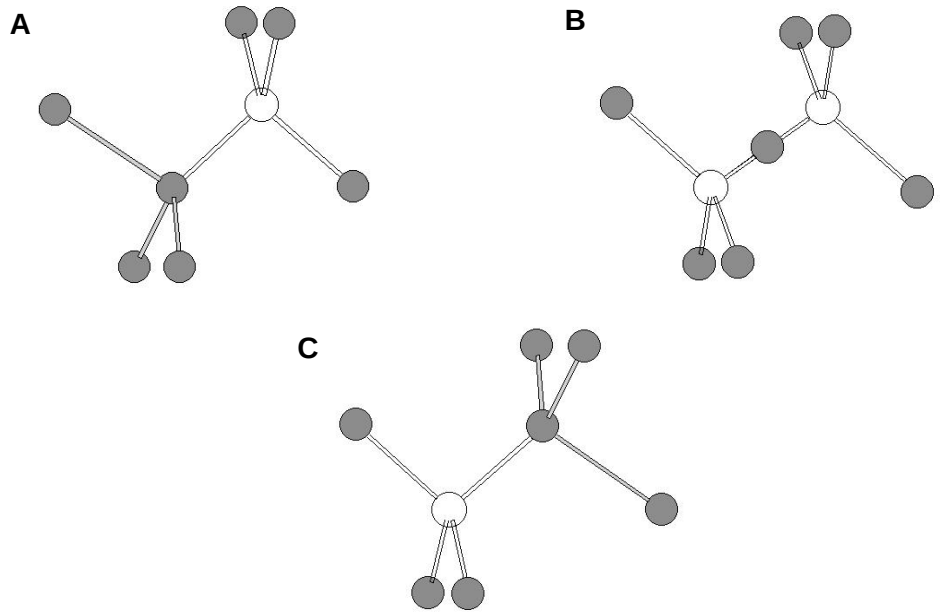

Fig. 4. Positions of the Si host atoms (gray circles) near the vacancy for the initial (A) and final (C) states and the saddle point (B) for diffusion. The vacant sites are shown by white circles.

3.3. Divacancy

3.3.1. Introduction

The divacancy (V_2) can be formed by pairing of two monovacancies during their migration in the lattice or alternatively in a single collision event upon irradiation by high energetic particles (electrons, neutrons, ions, etc.) [4,32]. The extensive treatment of the V_2 defect in silicon was done by EPR [4]. It was shown that the divacancy in Si could appear in four different charge states, positive V_2^+, neutral V_2^0, negative V_2^-, and doubly negative V_2^{2-}. The following structure was proposed for the V_2 (Fig. 5(a)): initially there are six broken bonds around the divacancy, one for each of the six Si atoms neighboring it. Atoms 1 and 2 pull together to form a "bent" pair bond as do the atoms 4 and 5. In its undistorted state the divacancy possess D_{3d} symmetry and induces two non-degenerate levels, a_{1g} and a_{1u}, in the valence band manifold and two doubly degenerate levels, e_u and e_g, inside the band gap. As a result of the degeneracy associated with filling the orbitals by electrons, Jahn-Teller distortion occurs which leads to lowering the lattice symmetry to C_{2h} and

splitting each of e level on two singlets, producing the four levels a_u, b_u, a_g and b_g (Fig.5(b)). It was found from EPR and recently supported theoretically [19,33,34] that degree of pairing distortion, that occur between atoms 1, 2 and 4, 5, is strong enough for the upper a_g level to go below the a_u level. The correct levels ordering for V_2 in Si from ab-initio calculations was only obtained by using cluster method, which indicates that cluster calculations are more reliable in this case than supercell ones. As in the case of the single vacancy, the divacancy related lattice relaxations, associated with Jahn-Teller distortion, were found to be long-ranged and anisotropic along the zigzag chains of atoms that contain vacant site and perpendicular to the divacancy axis [19].

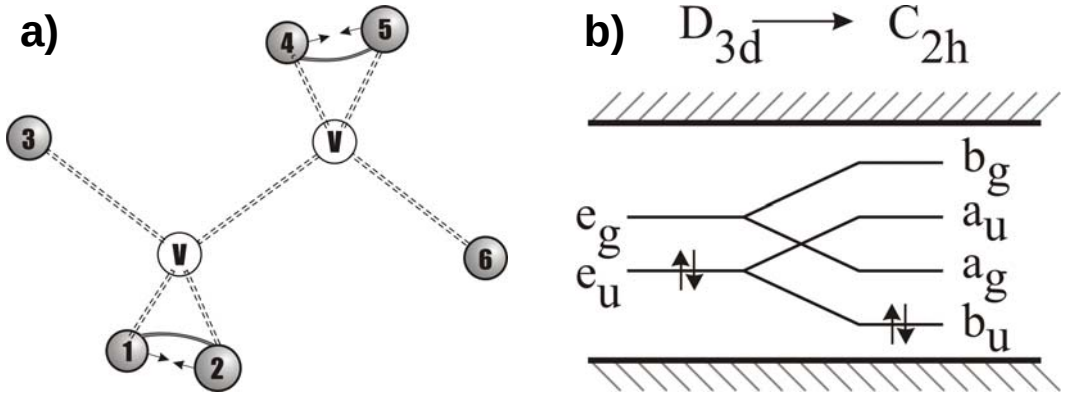

Fig. 5. a) Divacancy with its six neighbouring host atoms in Si. The pairing distortion of Si atoms and formation of new covalent bonds are sketched. b) Splitting of energy levels of divacancy in Si due to Jahn-Teller distorsion. The neutral charge state with two electrons in the gap level is shown.

The divacancy in silicon is stable up to ~220 °C. At higher temperatures it becomes mobile. At these temperatures the Fermi level is usually in the centre of the band gap, and divacancy is in the neutral charge state. It was found from EPR and infrared absorption studies that the neutral divacancy has the activation energy for migration of about 1.3 eV [4,5]. It was also shown that the divacancy can diffuse large distances in the lattice without dissociation, and that in oxygen rich crystals it can be trapped by interstitial oxygen atoms that results in the formation of V_2O defect [35-37]. The value for V_2 binding energy was estimated to be $\geq$ 1.6 eV. In a recent DLTS study [6] of the divacancy annealing and formation of V_2O complexes the same value for the activation energy of V_2 migration, 1.3

eV, was obtained as in earlier EPR and infrared absorption studies. It should be noted, however, that the available data in the literature for the activation energy of V_2 diffusion are spread in a rather wide range from 1.0 eV to 1.5 eV [4-7, 35].

It is believed that divacancy migrates through the jump of a neighbour Si atom to the vacant site with a saddle point in V-Si-V configuration. Based on ab-initio calculations [38] it was found that energy difference between V-V and V-Si-V states is 1.36 eV, that is, in a good agreement with the experimental data. The binding energy was calculated to be 1.74 eV.

3.3.2. Results of calculations and their discussion

It is thought that the divacancy diffuses through the one-step hopping of two adjacent vacancies with a saddle point in V-Si-V configuration [38]. This mechanism of diffusion has a simple justification. First, no sizable barrier for stabilizing the V-Si-V configuration at finite temperatures was found [38]. And second, the superposition of the vacancies strain fields, that causes an attractive interaction of two vacancies, results in a high energy barrier for dissociation of V_2. This implies that once two vacancies separate one lattice sites the probability of their joining back is higher than that of dissociation.

The only possibility to stabilize V-Si-V configuration is to do it technically by imposing constraints on the symmetry when the Si atom is placed in the centre of the cluster. The ground state energy for this configuration was found to be 1.82 eV higher than that for divacancy. AIMPRO allows to divide a migration path onto a few parts and then to generate a set of images between each pair of initial and final states in these parts separately. The two paths were generated with a set of seven images and then allowed to relax: first by linear interpolation between two separate configuration pairs: a) V-V-Si and V-Si-V, and b) V-Si-V and Si-V-V (Path I); and second by linear interpolation between two end positions (Path II). The first case represents the symmetrical diffusion path along ‹110› direction with identical V-V-Si → V-Si-V and V-Si-V → Si-V-V parts. As it was expected, in this case the diffusion barrier was found to be 1.82 eV, equal to the difference between the ground state energy of the saddle point in V-Si-V configuration and that of divacancy. If this representation is correct and corresponds to the MEP for divacancy diffusion, the Path II should obviously come to the same result. However for the Path II the

diffusion barrier was found to be 1.74 eV. This may indicate that: first, the diffusion path is not fully symmetrical along the ‹110› direction, and second, the considered paths along the ‹110› direction are not the minimum energy paths for the divacancy diffusion. The second assumption will be discussed later. The total energy variation along the diffusion path (Path II) and atomic configurations for the initial and final positions and the saddle point are represented in Fig. 6 and Fig. 7 respectively. From Fig. 7B one can see that in the saddle point configuration the central Si atom is displaced significantly from the position of an ideal lattice site. The distance between the position of this Si atom and the nearest ideal lattice site was found to be ~0.62 Å for Path II (Fig. 7B), which is ~26 % of ideal Si=Si bond, and ~0.27 Å for Path I.

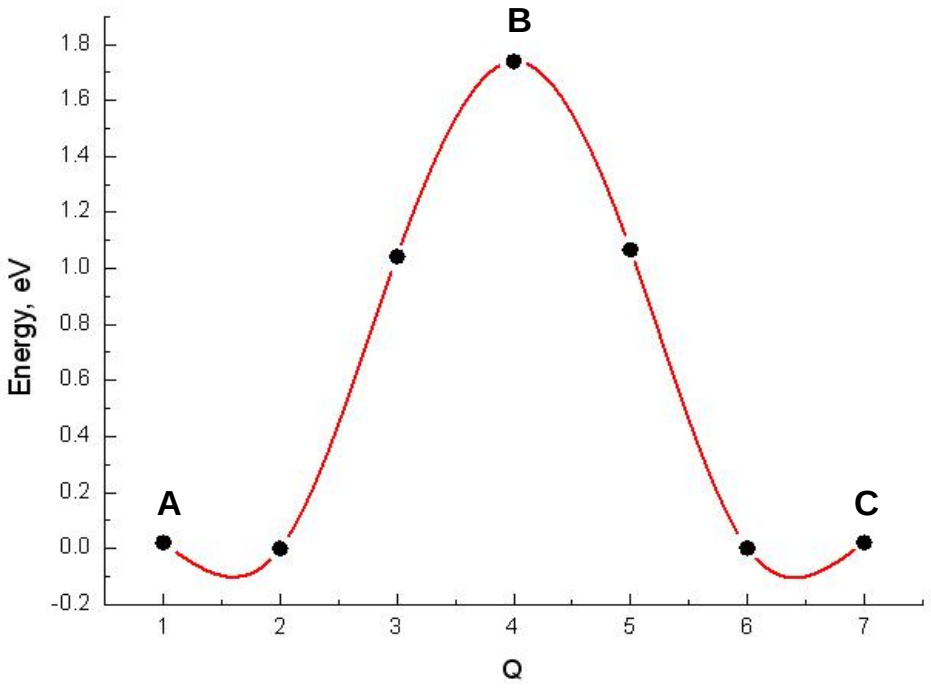

Fig. 6. The total energy variation along the diffusion path of a divacancy in a neutral charge state. Black circles correspond to the calculated energies of real atomic configurations relative to the energy of the initial position. The red solid line is an interpolation, which is shown as a guide for eyes. Positions A, B and C correspond to the atomic configurations shown in Fig. 7.

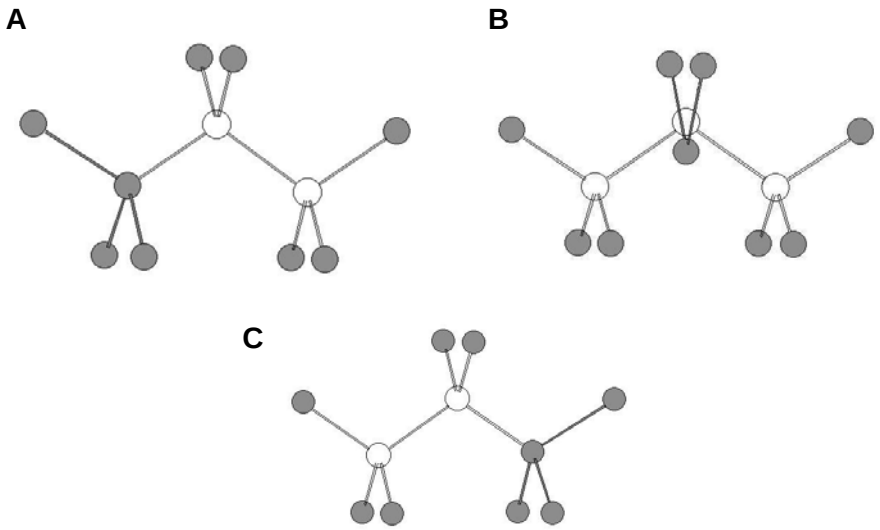

Fig. 7. Positions of the Si host atoms (gray circles) near the divacancy for the initial (A) and final (C) states and the saddle point (B) for diffusion. The vacant sites are shown by white circles.

The diffusion barrier for divacancy in Si obtained in this work and those found from experimental works and from previous LDA supercell calculations are shown in Table 2.

Table 2. Energy barrier for divacancy diffusion in a neutral charge state derived from experimental works and from ab-initio DFT calculations. All the values are in eV.

Experiment	DFT (supercell)	DFT (cluster)
1.3 [4,5], (1.5) [35]	1.36 [38]	1.74 (this work)

Possible reasons for the overestimation of the diffusion barrier value obtained in this work may be the same as in the case of single vacancy diffusion, i.e, too high value of the band gap energy in the cluster calculations and defect-surface interactions. For the single vacancy the overestimation is about 0.23 eV. In the case of divacancy this value is about 0.24 eV if compare with the highest experimental value for the diffusion barrier, 1.5 eV. A little bit higher error in the case of divacancy in comparison with that for the single vacancy calculations should be expected as a result of increasing effect of defect-surface interaction.

Other possible reason for the too high value of diffusion barrier obtained could be related to a possibility that the considered diffusion path is not the correct one. It might be possible that the diffusing Si atom deviate from the (110) plane and forms extended weak bonds with three nearest Si atoms on one side of the (110) plane that contains the zigzag chain of atoms with the divacancy. Some preliminary calculations are seems to support this idea. But the detail investigation has not been performed yet and it is a topic for further investigation.

3.4. Trivacancy

3.4.1. Introduction

In comparison to the vacancy and divacancy, the information available on the structure, electronic and dynamic properties of trivacancy (V_3) in Si is rather limited. It is thought that the trivacancy, a higher order radiation-induced defect, could be introduced by irradiation of Si crystals with particles of rather high energy (electrons with E > 5 MeV, neutrons, ions, etc.). In neutron-irradiated Si crystals the A4 EPR signal was assigned to the trivacancy in a (110) planar configuration [39]. It was shown later in Ref. [3] that annealing behaviour of the trivacancy is very similar to that of V_2 in Si, i.e. the EPR signal assigned to V_3 disappeared upon isochronal annealing in the temperature range 250-300 ^{o}C as well as the EPR signals assigned to the V_2 did.

Recently E4 and E5 (or E4a and E4b) electron traps with energy levels at E_c - 0.35 eV and E_c - 0.45 eV were tentatively assigned to the V_3 defect [40]. These traps were observed in DLTS spectra of Si particle detector diodes irradiated with high energy particles. It was found that the E4 and E5 traps disappeared upon annealing in the temperature range 50-100 ^{o}C [40,41]. So, the annealing behaviour of the E4 and E5 is different from that of the EPR A4 signal, which was assigned earlier to the V_3, making the assignment of the E4 and E5 traps to the V_3 doubtful.

According to ab-initio calculations, the minimum energy configuration of the V_3 in Si could be a “part of the hexagonal ring” (PHR) configuration, which for the V_3 is three neighbouring vacancies in the same (110) plane [42,43]. However, it has been argued recently that the so-called “fourfold” configurations are lower in energy for the neutral V_3 to V_5 defects than the PHR ones [44]. This structure is obtained by removing six Si atoms

from the crystal and placing three in such a way that all atoms end four-fold coordinated. No clear experimental evidences for the existence of V_3 in the "fourfold" configuration has been presented until recently, and electronic and dynamic properties of the V_3 defect in both configurations are not well understood.

It has been argued in a recent DLTS study that in the neutral charge state V_3 is bistable, with the fourfold configuration being lower in energy than the (110) planar configuration. V_3 in the (110) planar configuration gives rise to two acceptor levels at E_c-0.36 eV and E_c-0.46 eV, (E4 and E5 traps), while in the fourfold configuration the defect has trigonal symmetry and possess an acceptor level at E_c-0.075 eV (E_{75} trap) [45]. The transformation of the V_3 from the (110) planar configuration to the fourfold coordinated one was found to occur in the temperature range 50-100 ^oC, in an agreement with the results presented in Refs. [40] and [41]. However, it was shown that an application of forward bias injection with a current density in the range 10-15 A/cm^2 for 20 minutes at 300 K to the irradiated p^+-n diodes, which previously were annealed in the temperature range 50 to 100^oC, resulted in the complete regeneration of the E4 and E5 peaks and also in the disappearance of the E_{75} trap. Furthermore, it was found from multiple experiments with the sequential annealing/injection treatments that the E4/E5 $\leftrightarrow$ E_{75} transformations, i.e. the transformations between the two configurations of the neutral V_3, are fully reversible.

It was also found that the V_3 became mobile in Si at temperatures higher than 200 ^oC and could be trapped by an oxygen atom that resulted in the appearance of a V_3O defect [45]. The V_3O center is only stable in the (110) planar configuration and gives rise to two acceptor levels at E_c-0.34 eV and E_c-0.455 eV. The activation energy of the V_3 to V_3O transformation was found to be 1.49 $\pm$ 0.07 eV, which is very close to the activation energy of the transformation of V_2 to V_2O, 1.48 $\pm$ 0.05 eV [45].

3.4.2. Results of calculations and their discussion

No investigations of the trivacancy diffusion mechanism have been performed earlier. From recent experimental results two main conclusions can be made: 1) most probably the trivacancy migrates in planar configuration, and 2) the mechanism of the trivacancy diffusion might be similar to that of the divacancy. Thus, it is reasonable to

assume that trivacancy migrates through hopping of a Si atom between vacant lattice sites. No stable configuration was found for a Si atom in possible positions along the diffusion path. Two schemes were used for calculations of the V_3 diffusion path: in the first scheme the path was generated by a linear interpolation with a set of nine images between the initial and final configurations (Path I); and in the second scheme the path was defined by four points, including the initial and final configurations and two configurations with a migrating Si atom in vacant site positions along the path, and then expanded by linear interpolation between each pair of nearest points to 10 images (Path II). All images except the two end configurations were then allowed to relax. As the complexity of the problem increases substantially in comparison with the single vacancy and divacancy cases, the convergence of the method decreases. This implies that more structural relaxations for each image are needed. As the total number of images has also been increased the calculations have become extremely time demanding.

The saddle point for V_3 diffusion was found to be a configuration, in which the migrating Si atom is in the center of a C_{2h} symmetric arrangement of four vacancies in the (110) planar configuration, Fig. 10C. As the Path II contains an even number of images, there is no image that represent the saddle point configuration. After several iterations were performed, the path was expanded again by linear interpolation between each pair of nearest points to 19 images. Each of the new images was then allowed to relax to the electronic ground state. This allows to consider the saddle point configuration, calculate its energy and obtain smoother diffusion profile. The total energy variation along the diffusion path (Path II) and corresponding positions of travelling Si atom are shown in Fig. 8 and Fig. 9 respectively. Both Path I and Path II give similar estimation for the diffusion barrier of a neutral V_3, ~2.2 eV.

The energy variation along the diffusion path of a trivacancy is quite different from those obtained for a single vacancy and divacancy diffusion. In the case of trivacancy a separate peak is observed when approaching the saddle point (Fig. 8). To exclude the possibility that this effect arises from the complexity and low convergence of the calculations, we carried out a C_{2h} symmetry-constrained atomic relaxation of structure shown in Fig. 10C. For this reason a new bond-centred cluster was constructed. The ground state energy for the diffusion saddle point configuration of V_3 was found to be 2.12 eV compared to that of the most stable planar V_3 configuration in the neutral charge state.

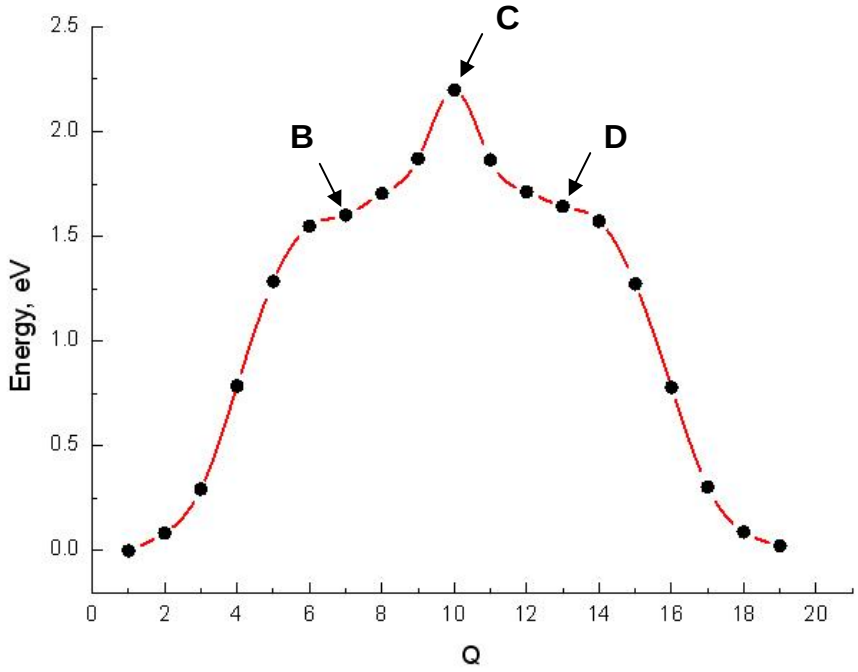

Fig. 8. The total energy variation along the diffusion path of a trivacancy in the neutral charge state. Black circles correspond to the calculated energies of real atomic configurations relative to the energy of the initial position. The red solid line is an interpolation, which is shown as a guide for eyes. Positions B, C and D correspond to the atomic configurations shown in Fig. 10.

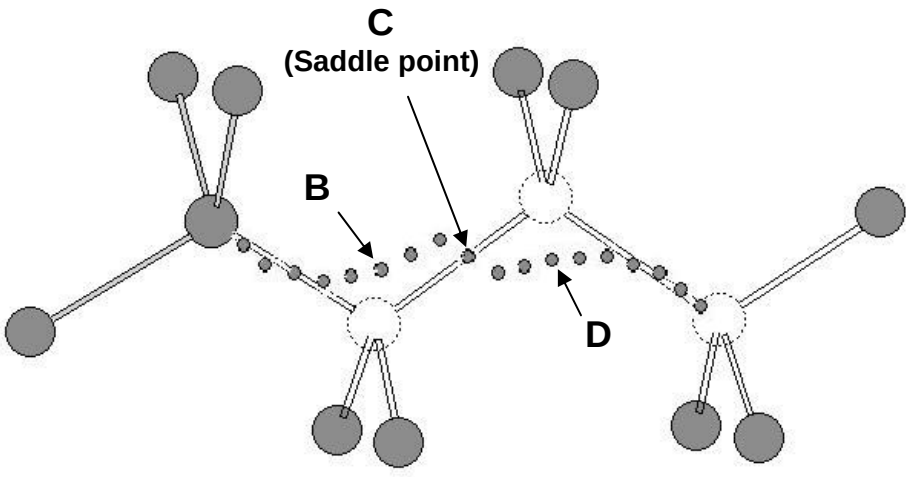

Fig. 9. Positions of a moving Si atom (shown by small grey circles) along the diffusion path for V_3. Positions B, C and D correspond to the atomic configurations shown in Fig.10.

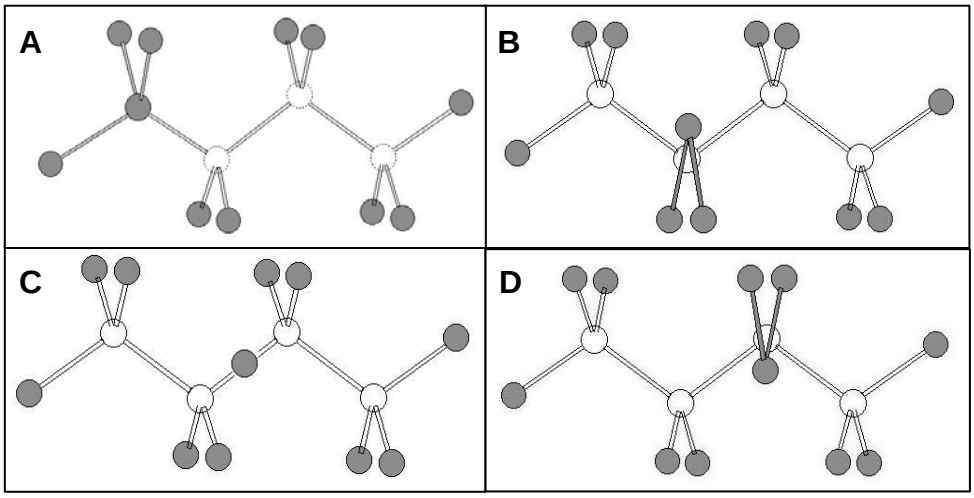

Fig. 10. The atomic configurations corresponding to four positions of travelling Si atom along the diffusion path for V_3. Figure **A** represents the initial configuration, and **C** – the saddle point configuration.

This value is quite similar to that obtained from the NEB calculations. However, the obtained value for diffusion barrier is much higher than the estimated experimental one, 1.49 eV. Even if one takes into account an overestimation of ~0.25 eV, comparable to those for the single vacancy and divacancy, the barrier is overestimated by about 0.4 eV. There might be several reasons for this overestimation.

1) The cluster is too small for a correct modelling of extended defects such as a trivacancy. During the V_3 diffusion large lattice distortions can occur, and the associated strain fields are not well accounted for in the present calculations.
2) The diffusion path is not symmetric or may deviate from (110) plane, as it was discussed for the case of divacancy. And the convergence of the NEB method is too slow to unravel these deflections at the present stage.
3) There might be some effects that we did not account for properly: e.g., the trivacancy migrates not in the neutral charge state; or capture-emission processes of charge carriers at different stages of diffusion can lead to a substantial decrease in the diffusion barrier.
4) When approaching the saddle point position some reversible configuration transformations may occur with possible lowering in the diffusion barrier. The backward transformations can be induced by capture or emission of charge carriers.

If the diffusion process is governed by some enhanced mechanisms (such as those discussed in 3) and 4) above) it is possible that there will be no saddle point in the configuration that is found for the diffusion by hopping of a Si atom between vacant sites in planar configuration.

We have also tried to investigate a diffusion mechanism for which the diffusion of trivacancy occurs through motion of a dimmer of Si atoms. The value of diffusion barrier for the dimmer motion and rotation in (110) and (010) planes was found to be higher than 2.4 eV. It was also found that a configuration Si-V-V-Si-Si-V-Si is stable with the ground state energy of 1.81 eV higher than that for the most stable C_{2v} configuration of trivacancy. This value can be considered as a lowest estimation of the binding energy of V_3.

There are still a lot of unresolved questions regarding the diffusion mechanism of trivacancy and further experimental and theoretical studies are required to achieve good understanding of the diffusion process of V_3 in Si.

SUMMARY

Based on first principle calculations an investigation of the diffusion processes of small vacancy clusters V_n (n = 1,2,3) in Si was performed. The calculated diffusion barriers are shown in Table 3 together with the corresponding experimental values. The detailed discussion of the results obtained was presented in Chapter 3 of the thesis. Here a short overview is given.

Table 3. Calculated in this work and experimental values of diffusion barriers (in eV) for the neutral V_n defects (n=1,2,3) in silicon. The overestimation of calculated values is also shown.

Method	**V_1**	**V_2**	**V_3**
Experiment	0.45[a]	1.3[b] (1.5)[c]	1.5[d]
DFT cluster [e]	0.68	1.74	2.2
Overestimation	0.23	0.24	0.7

[a] Ref. [24], [b] Ref. [4,5], [c] Ref. [35], [d] Ref. [45]

[e] This work

In the simplest case of single vacancy diffusion in the neutral charge state the activation energy was found to be 0.68 eV. This value is about 0.23 eV higher than that obtained experimentally [24,25]. It implies that some errors occur in the calculations, which may result from the defect-surface interaction and/or from the overestimation of the band gap energy in cluster calculations.

For the symmetrical diffusion path of divacancy in ‹110› direction with the V-Si-V saddle point configuration, which has been reported in literature [38], the diffusion barrier was found to be 1.82 eV. However, when the moving Si atom was not restricted from going through the vacant lattice site in the saddle point configuration, the lower barrier was obtained, 1.74 eV. This may indicate that the diffusion path is not fully symmetrical along the ‹110› direction. If one assumes the computational errors to be similar to those found in the single vacancy calculations, the obtained values for the diffusion barrier are comparable with the highest experimentally determined one, 1.5 eV. It was also found that in the saddle point configuration the moving Si atom is displaced significantly from the

position of ideal lattice site for about ~0.62 Å in the $\langle 00\bar{1} \rangle$ direction in the case where the saddle point energy of 1.74 eV was obtained, This displacement is about 26 % of the length of the ideal Si–Si, bond. Such a strong displacement has not been discussed in literature before. For the symmetrical diffusion path the displacement was found to be only ~0.27 Å. Furthermore, some preliminary calculations indicate that there might be other paths for divacancy diffusion, where the moving Si atom deviate from the (110) plane and in the saddle point forms extended weak bonds with three nearest Si atoms on one side of the (110) plane. An examination of this mechanism is a topic for further investigation.

Our results on the diffusion of trivacancy in Si can be considered as one of the first attempts to find the diffusion path and to determine the diffusion barrier of this defect. A possible diffusion path of V_3 in (110) plane was proposed and the saddle point configuration was found. However, the obtained value of the energy barrier for migration of the V_3 in Si, about 2.2 eV, seems to be overestimated. So, further efforts are necessary to correct the diffusion path and the value of energy barrier. The most probable reasons for the overestimation were discussed in the text. It was also found that the planar (110) configuration Si-V-V-Si-Si-V-Si is stable with the ground state energy of 1.81 eV higher than that for the most stable C_{2v} configuration of trivacancy.

Although, the cluster method is thought to be more reliable for calculations of vacancy type defects, we are going to perform similar calculations using supercell method to elucidate the possible disadvantages of each method and sources of errors that occur in the calculations.

The work performed provides a further insight into understanding the diffusion processes of small vacancy clusters in silicon and creates a basis for further investigations.

REFERENCES

1. G.D. Watkins, *J. Appl. Phys.* **103**, 106106 (2008).
2. H. Bracht and A. Chroneos, *J. Appl. Phys.* **104**, 076108 (2008).
3. J.W. Corbett, J.C. Bourgoin, L.J. Cheng, J.C. Corelli, Y.H. Lee, P.M. Mooney, and C. Weigel, in *Radiation Effects in Semiconductors 1976* (Inst. Phys. Conf. Ser. 31, Bristol and London, 1976) p. 1.
4. G.D. Watkins and J.W. Corbett, *Phys. Rev.* **138**, A543 (1965).
5. L.J. Cheng, J.C. Corelli, J.W. Corbett, and G.D. Watkins, *Phys. Rev.* **152**, 761 (1966).
6. M. Mikelsen, E.V. Monakhov, G. Alfieri, B.S. Avset, and G.G. Svensson, *Phys. Rev. B* **72**, 195207 (2005).
7. R. Poirier, V. Avalos, S. Dannefaer, F. Schiettekatte, and S. Roorda, *Physica B* **340-342**, 609 (2003).
8. H. Jonsson, G. Mills and K. W. Jacobsen, *Classical and Quantum Dynamics in Condensed Phase Simulations*, edited by B. J. Berne, G. Cicotti, and D. F. Coker, p.385 (World Scientific, Singapore, 1998).
9. G. Henkelman and H. Jonsson, *J. Chem. Phys*. **113**, 9978 (2000).
10. G. Henkelman, B. P. Uberuaga, and H. Jonsson, *J. Chem Phys.* **113**, 9901 (2000).
11. P. Hohenberg and W. Kohn, *Phys. Rev.* **136**, 864 (1964).
12. W. Kohn and L. J. Sham, *Phys. Rev.* **140**, A1133 (1965).
13. P. R. Briddon and R. Jones, *Phys. Stat. Sol.* (b) **217**, 131 (2000).
14. J. P. Perdew and Y. Wang, *Phys. Rev.* B **45**, 13244 (1992).
15. S. Goedecker, M. Teter and J. Hutter, *Phys. Rev*. B **54**, 1703 (1996).
16. G. B. Bachelet, D. R. Hamann and M. Schlüter, *Phys. Rev.* B 26, 4199 (1982).
17. R. W. Godby, M. Schluter, L. J. Sham, *Phys. Rev. Lett.* **56**, 2415 (1986)].
18. H. Jahn and E. Teller, *Proc. of the Royal Society of London. Series A, Math. And Physical Sciences* **161** (905), 220 (1937).
19. S. Öğüt and J.R. Chelikowski, *Phys. Rev. B* **64**, 245206 (2001).
20. R. Jones and P. R. Briddon, in *Indetification of Defects in Semiconductors*, edited by M. Stavola, volume 51A of *Semiconductors and Semimetals* (Academic Press, 1999).
21. Yaojun A. Du, Stephen A. Barr, Kaden R. A. Hazzard, Thomas J. Lenosky, Richard G. Hennig, and John W. Wilkins, *Phys. Rev. B* **72**, 241306 (R) (2005).

22. W. Windl, M. M. Bunea, R. Stumpf, S.T. Dunhan, and M. P. Masquelier, *Phys. Rev. Lett.* **83**, 4345 (1999).
23. G.D. Watkins, in *Radiation Damage in Semiconductors* (Dunod, Paris, 1964) p. 97.
24. G.D. Watkins, in *Lattice Defects in Semiconductors 1974* (Inst. Phys. Conf. Ser. 23, London, 1975) p. 1.
25. G.D. Watkins, in *Deep Centers in Semiconductirs,* ed. by S.T. Pantelides (Gordon and Breach, New York, 1986) p. 176.
26. G.A. Baraff, E.O. Kane, and M. Schluter, *Phys. Rev. B* **21**, 5662 (1980).
27. A. Antonelli, E. Kaxiras, and. D.J. Chadi, *Phys. Rev. Lett.* **81**, 2088 (1998).
28. G.D. Watkins and J.R. Troxell, *Phys. Rev. Lett.* **44**, 593 (1980).
29. P.W. Anderson, *Phys. Rev. Lett.* **34**, 953 (1975).
30. S. Dannefaer, P. Mascher, and D. Kerr, *Phys. Rev. Lett.* **56**, 2195 (1986).
31. B.P. Uberuaga, Ph.D. thesis, University of Washington, 2000.
32. J.W. Corbett and G.D. Watkins, *Phys. Rev.* **138**, A555 (1965).
33. M. Pesola, J. van Boehm, S. Pöykkö, and R.M. Nieminen, *Phys. Rev. B* **58**, 1106 (1998).
34. R.R. Wixom and A.F. Wright, *Phys. Rev. B* **74**, 205206 (2006).
35. B.G. Svensson, K. Johnsson, D-X. Xu, J.H. Svensson, and L. Lindstrom, *Radiation Effects and Defects in Solids* **111-112**, 439 (1989).
36. V.P. Markevich, A.R. Peaker, S.B. Lastovskii, L.I. Murin, and J.L. Lindstrom, *J. Phys.: Condens. Matter* **15**, S2779 (2003).
37. Mikelsen, E.V. Monakhov, G. Alfieri, B.S. Avset, and B.G. Svensson, *Phys. Rev. B* **72**, 195207 (2005).
38. G.S. Hwang and W.A. Goddard III, *Phys. Rev. B* **65**, 233205 (2002).
39. Y.-H. Lee and J.W. Corbett, *Phys. Rev. B* **9**, 4351 (1974).
40. M. Ahmed, S.J. Watts, J. Matheson, A. Holmes-Siedle, *Nucl. Instr. Methods in Phys. Research A* **457**, 588 (2001).
41. J.H. Bleka, L.I. Murin, E.V. Monakhov, B.S. Avset, and B.G. Svensson, *Appl. Phys. Lett.* **92**, 132102 (2008).
42. J.L. Hastings and S. K. Estreicher, *Phys. Rev. B* **56**, 10215 (1997).
43. T.E.M. Staab, A. Sieck, M. Haugk, M.J. Puska, T. Fraunheim, and H.S. Leipner, *Phys. Rev. B* **65**, 115210 (2002).

44. D.V. Makhov and L.J. Lewis, *Phys. Rev. Lett.* **92**, 255504 (2004).
45. V.P. Markevich, private communication.
46. Semiconductors – Basic Data, Otfried Madelung ed. (Springer, Berlin, 1996), p.16-18.